Effective conductance method for the primordial recombination spectrum

Yacine Ali-Haïmoud*
Institute for Advanced Study, Einstein Drive, Princeton, New Jersey 08540
(Dated: November 20, 2012)

As atoms formed for the first time during primordial recombination, they emitted bound-bound and free-bound radiation leading to spectral distortions to the cosmic microwave background. These distortions might become observable in the future with high-sensitivity spectrometers, and provide a new window into physical conditions in the early universe. The standard multilevel atom method habitually used to compute the recombination spectrum is computationally expensive, impeding a detailed quantitative exploration of the information contained in spectral distortions thus far. In this work it is shown that the emissivity in optically thin allowed transitions can be factored into a computationally expensive but cosmology-independent part and a computationally cheap, cosmology-dependent part. The slow part of the computation consists in pre-computing temperature-dependent effective "conductances", linearly relating line or continuum intensity to departures from Saha equilibrium of the lowest-order excited states ($2s$ and $2p$), that can be seen as "voltages". The computation of these departures from equilibrium as a function of redshift is itself very fast, thanks to the effective multilevel atom method introduced in an earlier work. With this factorization, the recurring cost of a single computation of the recombination spectrum is only a fraction of a second on a standard laptop, more than four orders of magnitude shorter than standard computations. The spectrum from helium recombination can be efficiently computed in an identical way, and a fast code computing the full primordial recombination spectrum with this method will be made publicly available soon.

I. INTRODUCTION

A significant part of our knowledge about the universe at early times and on large distance scales is derived from the observation and analysis of its spatial inhomogeneities. In particular, observations of the temperature and polarization anisotropies of the cosmic microwave background (CMB) have allowed cosmologists to determine the geometry, contents, and initial conditions of the universe to an exquisite level of precision (see for example Ref. [1]).

Additional, and perhaps complementary information, is hidden in the tiny but unavoidable spectral distortions to the nearly perfectly thermal radiation background [2, 3]. On the one hand, broad spectral distortions can be generated by energy injection in the early universe, taking the form of chemical potential ($\mu-$type) or Compton ($y-$type) distortions (and more generally continuously interpolating between these two analytic cases [4]), depending on the redshift of energy injection. Physical mechanisms causing such energy injections include the dissipation of small-scale acoustic waves, which occurs in the standard cosmological picture (see e.g. [5]), and possibly the decay or annihilation of dark matter into standard model particles that then deposit their energy into the primeval plasma [6]. A vast literature exists on the subject, and we refer the interested reader to the recent works [4, 7, 8] and references therein.

On the other hand, the primordial recombinations of helium and hydrogen lead to a few distortion photons per atom, in the form of free-bound and bound-bound photons. The seminal papers on primordial recombination by Peebles and Zeldovich et al. [9, 10] already evaluated the distortion due to Ly-α transitions and $2s-1s$ two-photon decays. Even though this represents a large distortion to the Wien tail of the CMB blackbody spectrum, it lies many orders of magnitude below the cosmic infrared background (CIB, [11]), which renders its detection very challenging, if not hopeless.

In addition, exactly one free-bound photon per hydrogen atom and two per helium atom were emitted, as well as a few bound-bound photons per atom from transitions between highly excited states[1] [12]. It was first pointed out by Dubrovich [13] that these primordial recombination lines could be observed today as broadened features in the centimeter to decimeter wavelength range. A few authors have since then tackled the computation of the recombination spectrum, with various degrees of approximation or numerical convergence [14–17], and it is only quite recently that highly-accurate computations were carried out by Rubiño-Martín, Chluba and Sunyaev [12, 18–20].

Thus far the study of the primordial recombination spectrum has remained the niche domain of a few aficionados. First and foremost, the observational prospects may seem meager, as the predicted signal in the cm-wavelengths lies a billion times below the undistorted CMB spectrum, far below the current best upper bounds on spectral distortions from FIRAS [21]. In addition, galactic and extragalactic foregrounds would need to be

* yacine@ias.edu

[1] Throughout this paper we refer to bound-bound transitions between "highly excited" states as those for which the lower state itself is excited, $n' \to n \geq 2$.

understood and subtracted very precisely. Finally, the machinery required to compute a recombination spectrum with the standard multilevel method is, although conceptually not very difficult, somewhat cumbersome to implement and too computationally expensive for a systematic analysis of its information content.

The reward in finding such a needle-in-a-haystack signal is, however, potentially significant. Ref. [22] showed that the recombination spectrum is a sensitive thermometer and baryometer. It could also provide a clean measurement of the primordial helium abundance, before the formation of the first stars [3, 20]. Finally, pre-existing spectral distortions could lead to a significant increase of the recombination radiation even if the initial distortions are small in absolute value [15, 23]. The recombination spectrum could therefore be a probe of non-standard physics such as dark-matter annihilations [24].

Let us point out, in addition, that technological advances should make it possible to reach sensitivities three orders of magnitude below that of FIRAS, corresponding to distortions at the level of $\sim 10^{-8}$ (see the proposal for the PIXIE instrument [25]). Spectral distortions from recombination are only one order of magnitude weaker than this sensitivity (and even get to the 10^{-8} level around 10 GHz [12]), and it is not unlikely that they will be within reach of the next generation instruments. The feasibility of foreground subtraction at the required level has yet to be demonstrated, but one may hope that the spatial isotropy of the signal and its very specific spectral features should allow us to disentangle it from foreground emission.

Before any of the truly challenging issues of instrumental sensitivity and foreground subtraction are addressed, it seems that the first task is to undertake a detailed quantitative study of the information content of the recombination spectrum. In order to do so, a *fast* and accurate computational method is required, so that the large space of cosmological parameters can be efficiently explored[2]. Introducing such a fast method is the purpose of the present work.

The main task in obtaining the spectrum resides in computing the populations of the excited states, or, more precisely, their small departures from equilibrium with one another, since the line and continuum emissions are proportional to the latter. High-precision spectra require accounting for excited states up to principal quantum number $n_{\rm max}$ of a few hundred, resolving the angular momentum substates. With the standard multilevel atom method, one has to invert a large $\frac{n_{\rm max}^2}{2} \times \frac{n_{\rm max}^2}{2}$ matrix at each timestep in order to compute the populations of the excited states (although this matrix is sparse due to selection rules, so only $\mathcal{O}(n_{\rm max}^3)$ elements are nonzero). Currently the fastest code using this method takes about one hour for $n_{\rm max} = 100$ and one full day for $n_{\rm max} = 250$ on a standard laptop, with the computation time scaling as $t \propto n_{\rm max}^{3.7}$ [28].

The method that we introduce here allows us to factorize the problem into a computationally expensive part (for which large linear systems need to be solved) that is cosmology-independent and can be pre-computed once and for all, and a computationally cheap part that does depend on cosmology. This method builds on and extends the effective multilevel atom (EMLA) method introduced in an earlier work [29] (hereafter AH10; see also Refs. [30, 31]); it is, however, not a trivial extension, since the EMLA method is designed for computing the free electron fraction $x_e(z)$ and essentially collapses all the transitions between excited states into effective transition rates into and out of $2s$ and $2p$. In this process, information not directly necessary to the evolution of the free electron fraction is lost, whereas our present goal is to go beyond $x_e(z)$ and compute the full recombination spectrum.

We shall lay down our method in detail in the remainder of this paper, but the main idea can be intuitively understood if one pictures the system of radiatively connected excited levels as a circuit, where the currents are the line intensities, the voltages are the departures of the excited states populations from Saha equilibrium, and the conductances are the transition rates (this insightful analogy is due to Chris Hirata [32]). The linearity of Kirchhoff's laws (the steady-state rate equations for the excited state) ensures that the "current" in any transition is proportional to the outer "voltages", i.e. the departures from Saha equilibrium of the $2s$ and $2p$ states. The proportionality coefficients, which we shall call effective conductances, moreover only depend on the temperature of the ambient blackbody radiation that is nearly undistorted at the relevant frequencies (this can in principle be generalized to include simple parameterizations of the ambient spectrum, as well as collisional transitions). Once the effective conductances are pre-computed as a function of transition energy and temperature, the recombination spectrum can be computed very efficiently for any cosmology, by using the EMLA method to evaluate the recombination history and the outer "voltages" as a function of redshift. This method is very similar in spirit to the widely used line-of-sight integration method for CMB anisotropies [33], which factorizes the computation of the CMB power-spectrum into a geometric, cosmology-independent part and a cosmology-dependent but multipole-independent source term. We illustrate our method graphically in Fig. 1.

This paper is organized as follows. In Sec. II, we write down the general equations that need to be solved for the computation of the recombination spectrum. The effective conductance method is described in Sec. III. We discuss our numerical implementation and results in Sec. IV and give our conclusions and future research directions in Sec. V.

[2] It was brought to my attention by J. Chluba that Fendt [26] conducted a preliminary study of cosmological parameter estimation from spectral distortions, using the fast interpolation algorithm Pico [27].

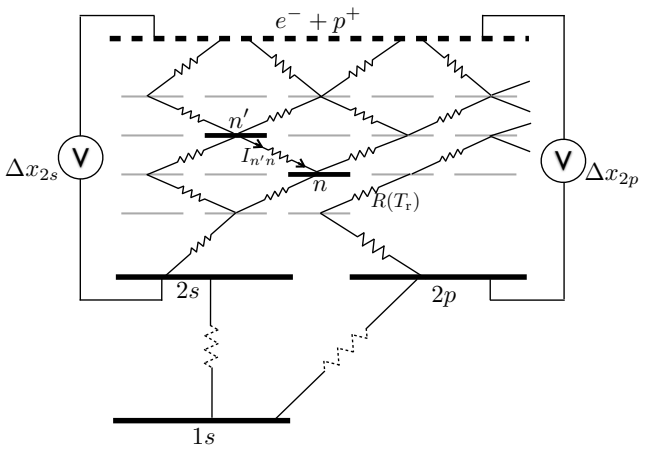

FIG. 1. Schematic representation of the main idea of this paper, highlighting the circuit analogy of Hirata [32]. All transitions between excited states are mediated by blackbody photons and their rates (and corresponding resistances $R(T_\mathrm{r})$ shown as solid resistor symbols) only depend on the blackbody temperature. The linearity of the steady-state rate equations (Kirchhoff's laws in the circuit analogy) ensures that the current $I_{n'n}$ in any transition between excited states is linear in the departures from Saha equilibrium Δx_{2s} and Δx_{2p}, which play the role of externally imposed voltages. The proportionality coefficient is a function of temperature only. The values of Δx_{2s} and Δx_{2p} are determined from the balance between the net downward current from the highly excited states (obtained through the effective rates defined in AH10) and the non-thermal transition rates to the ground state (represented by dashed resistor symbols). We have not represented all allowed transitions in order to keep the graph readable.

II. GENERAL EQUATIONS

A. Notation

We denote by n_H the total number density of hydrogen in all its forms (ionized and neutral), x_e the ratio of the free-electron abundance to the total hydrogen abundance, x_p the fraction of ionized hydrogen, and x_{nl} (or in some cases X_{nl}) the fractional abundance of neutral hydrogen in the excited state of principal quantum number n and angular momentum number l. The matter and radiation temperatures are denoted by T_m and T_r, respectively. We denote emissivities by j_ν (with units of energy per unit time per frequency interval per unit volume per unit solid angle) and specific intensities by I_ν (with units of energy per unit time per frequency interval per unit area per unit solid angle). All our derivations are for hydrogen atoms but the generalization to helium is straightforward. We only consider radiative transitions here and neglect the effect of collisions.

B. Bound-bound emission from transitions between excited states

The emissivity due to bound-bound transitions between excited states is given by

$$j_\mathrm{bb}(\nu) = n_\mathrm{H}\frac{h\nu}{4\pi}\times \sum_{2\leq n<n'}\sum_{l,l'}\left[x_{n'l'}R_{n'l'\rightarrow nl} - x_{nl}R_{nl\rightarrow n'l'}\right]\delta(\nu-\nu_{n'n}), \quad (1)$$

where $\nu_{n'n}$ is the frequency of the $n'l'\rightarrow nl$ transitions and $R_{nl\rightarrow n'l'}$ represents the radiative transition rate from nl to $n'l'$. The recombination process adds at most a few photons per atom, and the transitions between excited states are mostly below the peak of the blackbody spectrum (except for Balmer transitions, but their energy is only a few times above the blackbody peak, where there is still a very large number of thermal photons per hydrogen atom). As a consequence, the radiation field mediating the transitions is, to $\sim 10^{-8}$ accuracy, a blackbody at temperature T_r. One can check the validity of this assumption a posteriori once the distortions are computed (see for example Fig. 2 of Ref. [18]). Note, however, that small y-distortions to the blackbody spectrum (at the level of $y\sim 10^{-6}$) may significantly enhance the hydrogen and helium line emission [15, 23]. We defer the study of the effect of such pre-existing distortions on the recombination spectrum to future work, and shall here assume that transitions between excited states are mediated by thermal photons only.

With this assumption, the radiative transition rates satisfy the detailed balance relations,

$$R_{n'l'\rightarrow nl} = \frac{q_{nl}}{q_{n'l'}}R_{nl\rightarrow n'l'}, \quad (2)$$

where we have defined

$$q_{nl}\equiv(2l+1)\mathrm{e}^{-E_n/kT_\mathrm{r}}, \quad (3)$$

where $E_n\equiv -13.6\ \mathrm{eV}/n^2$ is the (negative) energy of the bound states with principal quantum number n.

We see that if the excited states were in Boltzmann equilibrium, so that $x_{n'l'}/x_{nl} = q_{n'l'}/q_{nl}$, the net emissivity would vanish. The emissivity therefore scales linearly with the small departures from equilibrium. To make this apparent, let us define the departures from Saha equilibrium at temperature T_r with the free electron and protons,

$$\Delta x_{nl}\equiv x_{nl} - \frac{q_{nl}}{q_e}n_\mathrm{H}x_e x_p, \quad (4)$$

where we have defined

$$q_e\equiv\left(\frac{2\pi m_e kT_\mathrm{r}}{h^2}\right)^{3/2}, \quad (5)$$

where m_e is the reduced mass of the electron-proton system. We can now rewrite the bound-bound emissivity in

the following form:

$$j_{\rm bb}(\nu) = n_{\rm H}\frac{h\nu}{4\pi}\times \sum_{2\le n<n'}\sum_{l,l'}\left[\frac{q_{nl}}{q_{n'l'}}\Delta x_{n'l'} - \Delta x_{nl}\right] R_{nl\to n'l'}\delta(\nu-\nu_{n'n}), \quad (6)$$

where the Saha-equilibrium pieces have cancelled out.

C. Free-bound emission

The emissivity due to free-bound transitions to excited states is given by

$$j_{\rm fb}(\nu) = n_{\rm H}\frac{h\nu}{4\pi}\sum_{n\ge 2}\sum_{l<n}\left[n_{\rm H}x_e x_p\frac{d\alpha_{nl}}{d\nu} - x_{nl}\frac{d\beta_{nl}}{d\nu}\right], \quad (7)$$

where $d\alpha_{nl}/d\nu$ is the differential recombination coefficient per frequency interval of the emitted photon and $d\beta_{nl}/d\nu$ is the differential photoionization rate per frequency interval of the ionizing photon. Recombinations of the thermal electrons and protons to the excited states are mediated by blackbody photons; as a consequence, $d\alpha_{nl}/d\nu$ and $d\beta_{nl}/d\nu$ are related through the relation (see for example Eq. (2) of AH10):

$$\frac{d\alpha_{nl}}{d\nu} = \left(\frac{T_{\rm r}}{T_{\rm m}}\right)^{3/2}\exp\left[(h\nu+E_n)\left(\frac{1}{kT_{\rm r}}-\frac{1}{kT_{\rm m}}\right)\right] \times \frac{q_{nl}}{q_e}\frac{d\beta_{nl}}{d\nu}. \quad (8)$$

We have purposefully made the ratio and difference of the matter and radiation temperatures appear in this expression. At high redshifts when the recombination spectrum is emitted, the matter temperature is locked to the radiation temperature by Compton heating (see for example Ref. [34]). Computing the coupled evolution of the ionization history and matter temperature with HyRec[3] [35], we find that the fractional difference between the two temperatures is less than 10^{-5} for $z \gtrsim 1100$ and less than 10^{-3} for $z \gtrsim 800$. We can therefore Taylor-expand the above expression in the small parameter $\Delta T/T \equiv (1 - T_{\rm m}/T_{\rm r})$ (note that with this convention $\Delta T > 0$ for $T_{\rm m} < T_{\rm r}$) and obtain

$$\frac{d\alpha_{nl}}{d\nu} \approx \frac{q_{nl}}{q_e}\frac{d\beta_{nl}}{d\nu}\left[1+\left(\frac{3}{2}-\frac{h(\nu-\nu_{cn})}{kT_{\rm r}}\right)\frac{\Delta T}{T}\right] \equiv \frac{q_{nl}}{q_e}\frac{d\beta_{nl}}{d\nu}\left[1+\gamma_n(\nu)\frac{\Delta T}{T}\right], \quad (9)$$

where $\nu_{cn} \equiv -E_n/h$ is the photoionization threshold from the n-th shell and the second expression defines the dimensionless parameter $\gamma_n(\nu)$. Again, we see that the free-bound emissivity would vanish if the excited states were in Saha equilibrium with the ionized plasma and if the matter and radiation temperature were identical. We can rewrite the free-bound emissivity in terms of small departures from equilibrium as follows:

$$j_{\rm fb}(\nu) = n_{\rm H}\frac{h\nu}{4\pi}\times \sum_{n\ge 2}\sum_{l<n}\left[\frac{q_{nl}}{q_e}n_{\rm H}x_e x_p\gamma_n(\nu)\frac{\Delta T}{T} - \Delta x_{nl}\right]\frac{d\beta_{nl}}{d\nu}. \quad (10)$$

D. Radiative transfer equation

Strictly speaking, the computation of the specific intensity requires the knowledge of not only the emissivity but also the absorption coefficient [36]. However, the Sobolev optical depths of most bound-bound transitions are much lower than unity [37, 38], perhaps with the exception of the very high-n transitions ($n \gtrsim 300$), as can be seen from extrapolating Fig. 11 of Ref. [19]. It is possible that a proper accounting of the nonzero optical depth in very high-n transitions could lead to small modifications in the low-frequency part of the spectrum ($\nu \lesssim 0.1$ GHz); however, in that frequency range other effects that we are neglecting significantly affect the spectrum too, such as free-free absorption [19] and collisional transitions [28]. We shall therefore assume the optically-thin limit for all bound-bound transitions between excited states, as well as free-bound transitions.

The radiative transfer equation in the optically thin regime in an expanding homogeneous universe takes the simple form

$$\frac{d}{dt}\left(\frac{I_\nu}{\nu^3}\right) \equiv \left[\frac{\partial}{\partial t}\left(\frac{I_\nu}{\nu^3}\right) - H\nu\frac{\partial}{\partial\nu}\left(\frac{I_\nu}{\nu^3}\right)\right] = c\frac{j_\nu}{\nu^3}. \quad (11)$$

In between resonances (where $j_\nu = 0$), the quantity I_ν/ν^3 is conserved along a photon trajectory, so that

$$I_\nu(z) = \left(\frac{\nu}{\nu'}\right)^3 I_{\nu'}(z'), \quad (12)$$

where

$$1+z' = \frac{\nu'}{\nu}(1+z). \quad (13)$$

In the vicinity of a resonance line, $j_\nu = J_0\delta(\nu-\nu_0)$, the solution to the radiative transfer equation is

$$I^-_{\nu_0} = I^+_{\nu_0} + \frac{cJ_0}{H\nu_0}, \quad (14)$$

where $I^+_{\nu_0}$ and $I^-_{\nu_0}$ are the specific intensities at the blue and red sides of the resonant line, respectively.

The general solution of the radiative transfer equation can be written in the following integral form

$$I_\nu(z) = c\int_\nu^\infty d\nu'\left(\frac{1+z}{1+z'}\right)^3\frac{j_{\nu'}}{H\nu'}\Big|_{z'} = c\, n_{\rm H}(z)\int_\nu^\infty\frac{d\nu'}{H\nu'}\frac{j_{\nu'}}{n_{\rm H}}\Big|_{z'}, \quad (15)$$

[3] http://www.sns.ias.edu/∼yacine/hyrec/hyrec.html

where the redshift z' and frequency ν' are related through Eq. (13) and we used the fact that $n_{\rm H}(z) \propto (1+z)^3$.

III. THE EFFECTIVE CONDUCTANCE METHOD

A. Populations of the excited states

In order to obtain the bound-bound and free-bound emissivities, we see that we need to evaluate the populations of the excited states, or, more precisely, their small departures from Saha equilibrium with the plasma.

The populations of excited states can be obtained to very high accuracy in the steady-state approximation, because of the large ratio of internal transition rates to the overall recombination rate. This assumption was checked explicitly in Ref. [28] and found to be extremely accurate, for the computation of both the recombination history and the recombination spectrum.

Following AH10, we separate the excited states in "interior" states, only connected radiatively to other excited states and the continuum, and "interface" states, essentially $2s$ and $2p$ (and potentially any additional "weak interface" states, such as $3s, 3p, 3d...$), which are radiatively connected to the ground state. We denote the populations of the former by a capital X_K, where K stands for both quantum numbers of the state, and those of the latter by x_i, where $i = 2s, 2p$ (and $3s, 3p, 3d...$ if needed).

The steady-state rate equation for the population of the interior state K is

$$0 \approx \dot{X}_K = n_{\rm H} x_e x_p \alpha_K + \sum_i x_i R_{i\to K} + \sum_{L\neq K} X_L R_{L\to K} - X_K \Gamma_K, \quad (16)$$

where $\alpha_K(T_{\rm m}, T_{\rm r})$ is the total recombination coefficient to the state K (accounting for stimulated recombinations) and

$$\Gamma_K \equiv \beta_K + \sum_{L\neq K} R_{K\to L} + \sum_i R_{K\to i} \quad (17)$$

is the total rate of transitions out of the state K, where β_K is the total photoionization rate from K. Note that here again we have assumed that the Sobolev escape probability is unity in all transitions (or that the Sobolev optical depth is zero). If this were not the case the net transition rates would depend non-linearly on the state populations, which would significantly complicate matters.

Provided the transitions between excited states are mediated by blackbody photons, the transition rates satisfy the detailed balance relation Eq. (2). The recombination coefficients and photoionization rates are related through

$$\alpha_K(T_{\rm m} = T_{\rm r}) = \frac{q_K}{q_e} \beta_K(T_{\rm r}). \quad (18)$$

We can now rewrite the system in terms of the small departures from Saha equilibrium with the continuum, and to linear order in $\Delta T/T$:

$$0 = -n_{\rm H} x_e x_p \Delta T \frac{\partial \alpha_K}{\partial T_{\rm m}}\Big|_{T_{\rm m}=T_{\rm r}} + \sum_i \Delta x_i R_{i\to K} + \sum_{L\neq K} \Delta X_L R_{L\to K} - \Delta X_K \Gamma_K. \quad (19)$$

In the standard multilevel atom method, the large system (19) is solved at every timestep, which makes the computation very slow.

Following AH10, we define the matrix $\boldsymbol{M}$ of elements

$$M_{KL} \equiv \Gamma_K \delta_{KL} - (1-\delta_{KL}) R_{K\to L}. \quad (20)$$

We also define the vector $\Delta\boldsymbol{X}$ of elements ΔX_K and the source vector $\Delta\boldsymbol{S}$ of elements

$$\Delta S_K \equiv -n_{\rm H} x_e x_p \Delta T \frac{\partial \alpha_K}{\partial T_{\rm m}}\Big|_{T_{\rm m}=T_{\rm r}} + \sum_i \Delta x_i R_{i\to K}. \quad (21)$$

The system (19) can be rewritten in compact matrix form as

$$\boldsymbol{M}^{\rm T}(\Delta\boldsymbol{X}) = \Delta\boldsymbol{S}, \quad (22)$$

where $\boldsymbol{M}^{\rm T}$ is the transpose of $\boldsymbol{M}$. We showed in AH10 that the matrix $\boldsymbol{M}$ is nonsingular, and this system has the formal solution

$$\Delta\boldsymbol{X} = (\boldsymbol{M}^{\rm T})^{-1}(\Delta\boldsymbol{S}) = (\boldsymbol{M}^{-1})^{\rm T}(\Delta\boldsymbol{S}), \quad (23)$$

i.e., explicitly,

$$\Delta X_K = \sum_L (\boldsymbol{M}^{-1})_{LK} \Delta S_L = -n_{\rm H} x_e x_p \Delta T \sum_L (\boldsymbol{M}^{-1})_{LK} \frac{\partial \alpha_L}{\partial T_{\rm m}}\Big|_{T_{\rm m}=T_{\rm r}} + \sum_i \Delta x_i \sum_L (\boldsymbol{M}^{-1})_{LK} R_{i\to L}. \quad (24)$$

We showed in AH10 that detailed balance relations between radiative transition rates ensure that

$$(\boldsymbol{M}^{-1})_{LK} = \frac{q_K}{q_L} (\boldsymbol{M}^{-1})_{KL}. \quad (25)$$

Using the detailed balance relation for $R_{i\to L}$, we may rewrite the last term of Eq. (24) as

$$\sum_L (\boldsymbol{M}^{-1})_{LK} R_{i\to L} = \frac{q_K}{q_i} \sum_L (\boldsymbol{M}^{-1})_{KL} R_{L\to i} \equiv \frac{q_K}{q_i} P_K^i, \quad (26)$$

where P_K^i is the probability that an excited atom initially in the interior state K eventually reaches the interface state i (after possibly many transitions in the interior), the complementary events being to eventually reach one

of the other interface states or to be photoionized. The probabilities P_K^i were defined in AH10, where they were an intermediate step to compute the effective recombination coefficients to and effective transition rates between the interface states. In the last line of Eq. (26), we have used the formal solution of the defining equation for the probabilities P_K^i.

Let us now deal with the first term of Eq. (24). We define the dimensionless coefficients

$$\gamma_K \equiv -\frac{\partial \log \alpha_K}{\partial \log T_\mathrm{m}}\Big|_{T_\mathrm{m}=T_\mathrm{r}}. \tag{27}$$

Using again detailed balance relations, we obtain

$$\begin{aligned}\sum_L (\boldsymbol{M}^{-1})_{LK} \frac{\partial \alpha_L}{\partial T_\mathrm{m}}\Big|_{T_\mathrm{m}=T_\mathrm{r}} &= -\frac{1}{T_\mathrm{r}}\frac{q_K}{q_e}\sum_L (\boldsymbol{M}^{-1})_{KL}\beta_L\gamma_L \\ &\equiv -\frac{1}{T_\mathrm{r}}\frac{q_K}{q_e}\tilde{P}_K^e, \end{aligned}\tag{28}$$

where the last equality *defines* the dimensionless coefficient $\tilde{P}_K^e$. If all the coefficients γ_L were equal to unity, then we would have $\tilde{P}_K^e = P_K^e$, the probability that an excited atom initially in the interior state K eventually gets photoionized before reaching an interface state. In general, however, $\gamma_L \neq 1$ (but is in general positive and of order unity), so the numbers $\tilde{P}_K^e$ do not have a clear physical significance but are numerically of the same order as the P_K^e.

We therefore end up with the following compact expression for the departures from Saha equilibrium:

$$\Delta X_K = \frac{q_K}{q_e}\tilde{P}_K^e n_\mathrm{H} x_e x_p \frac{\Delta T}{T} + \sum_i \frac{q_K}{q_i} P_K^i \Delta x_i. \tag{29}$$

Looking more closely at equation (29), we see that the departure from Saha equilibrium of any excited state is proportional to the difference between matter and radiation temperature (so long as this difference is small) times $n_\mathrm{H} x_e x_p$, and to the departures from Saha equilibrium of the small set of interface states. The proportionality coefficients are functions of radiation temperature only. If we *define* $P_j^i \equiv \delta_{ij}$ and $\tilde{P}_i^e \equiv 0$ for interface states i, j, we can write a general equation valid for any excited state (including the interface states) in the form

$$\Delta x_{nl} = \frac{q_{nl}}{q_e}\tilde{P}_{nl}^e n_\mathrm{H} x_e x_p \frac{\Delta T}{T} + \sum_i \frac{q_{nl}}{q_i} P_{nl}^i \Delta x_i. \tag{30}$$

B. Effective conductances

We can now rewrite the net decay rate in the $n' \to n$ transitions (with $n < n'$), per hydrogen atom, in the form

$$\begin{aligned}&\sum_{l,l'}\left[\frac{q_{nl}}{q_{n'l'}}\Delta x_{n'l'} - \Delta x_{nl}\right] R_{nl\to n'l'} \\ &= \mathcal{G}_{n'n}^e n_\mathrm{H} x_e x_p \frac{\Delta T}{T} - \sum_i \mathcal{G}_{n'n}^i \Delta x_i, \end{aligned}\tag{31}$$

where we have defined the coefficients

$$\mathcal{G}_{n'n}^e(T_\mathrm{r}) \equiv \sum_{l,l'}\frac{q_{nl}}{q_e}\left[\tilde{P}_{n'l'}^e - \tilde{P}_{nl}^e\right] R_{nl\to n'l'}, \tag{32}$$

$$\mathcal{G}_{n'n}^i(T_\mathrm{r}) \equiv \sum_{l,l'}\frac{q_{nl}}{q_i}\left[P_{nl}^i - P_{n'l'}^i\right] R_{nl\to n'l'}. \tag{33}$$

Note the minus sign in Eq. (31): we have chosen this convention because the excited states are in general underpopulated with respect to Saha equilibrium, and the coefficients $\mathcal{G}_{n'n}$ defined in Eq. (33) are positive (in general the probability of reaching interface states decreases as n increases).

If one thinks of the departures from Saha equilibrium Δx_i as voltages and of the net decay rate in the $n' \to n$ transitions as a current, then the coefficients $\mathcal{G}_{n'n}^i$ can be thought of as effective conductances linearly relating the two. A similar analogy can be made for the first term: there, the voltage is the fractional temperature difference $\Delta T/T$ and the conductance would be $n_\mathrm{H} x_e x_p \mathcal{G}_{n'n}^e$. Note that the $\mathcal{G}^e$ have units of cm^3 s^{-1} whereas the $\mathcal{G}^i$ have units of s^{-1}.

Similarly, the net free-bound decay rate per unit frequency can be rewritten as

$$\begin{aligned}&\sum_{n\geq 2}\sum_{l<n}\left[\frac{q_{nl}}{q_e} n_\mathrm{H} x_e x_p \gamma_n(\nu)\frac{\Delta T}{T} - \Delta x_{nl}\right]\frac{d\beta_{nl}}{d\nu} \\ &= \frac{d\mathcal{G}_\mathrm{fb}^e}{d\nu} n_\mathrm{H} x_e x_p \frac{\Delta T}{T} - \sum_i \frac{d\mathcal{G}_\mathrm{fb}^i}{d\nu}\Delta x_i, \end{aligned}\tag{34}$$

where we have defined the differential effective conductances

$$\frac{d\mathcal{G}_\mathrm{fb}^e}{d\nu} \equiv \sum_{n\geq 2}\sum_{l<n}\frac{q_{nl}}{q_e}\left[\gamma_n(\nu) - \tilde{P}_{nl}^e\right]\frac{d\beta_{nl}}{d\nu}, \tag{35}$$

$$\frac{d\mathcal{G}_\mathrm{fb}^i}{d\nu} \equiv \sum_{n\geq 2}\sum_{l<n}\frac{q_{nl}}{q_i} P_{nl}^i \frac{d\beta_{nl}}{d\nu}. \tag{36}$$

Here again we have defined the effective conductance $d\mathcal{G}_\mathrm{fb}^i/d\nu$ with a positive sign, such that the current is positive when the interface states are underpopulated with respect to Saha equilibrium.

C. Bound-bound and free-bound emissivities

The expressions for the emissivities can now be rewritten in terms of the effective conductances:

$$\begin{aligned}&j_\mathrm{bb}(\nu) = n_\mathrm{H}\frac{h\nu}{4\pi} \times \\ &\sum_{n<n'}\left[\mathcal{G}_{n'n}^e n_\mathrm{H} x_e x_p \frac{\Delta T}{T} - \sum_i \mathcal{G}_{n'n}^i \Delta x_i\right]\delta(\nu - \nu_{n'n}) \end{aligned}\tag{37}$$

$$j_\mathrm{fb}(\nu) = n_\mathrm{H}\frac{h\nu}{4\pi}\left[\frac{d\mathcal{G}_\mathrm{fb}^e}{d\nu} n_\mathrm{H} x_e x_p \frac{\Delta T}{T} - \sum_i \frac{d\mathcal{G}_\mathrm{fb}^i}{d\nu}\Delta x_i\right] \tag{38}$$

We can rewrite the total emissivity formally as

$$j_\nu \equiv j_{\rm bb}(\nu) + j_{\rm fb}(\nu) = n_{\rm H}\frac{h\nu}{4\pi}\times \left[\frac{d\mathcal{G}^e}{d\nu}(\nu,T_{\rm r})\; n_{\rm H}x_e x_p\frac{\Delta T}{T} - \sum_i \frac{d\mathcal{G}^i}{d\nu}(\nu,T_{\rm r})\Delta x_i\right], \quad (39)$$

where

$$\frac{d\mathcal{G}^{e,i}}{d\nu} \equiv \sum_{n<n'} \mathcal{G}^{e,i}_{n'n}\delta(\nu-\nu_{n'n}) + \frac{d\mathcal{G}^{e,i}_{\rm fb}}{d\nu}. \quad (40)$$

Equation (39), along with the definitions of effective conductances given above, constitutes the fundamental result of this paper. What it means is that the emissivity can be factored into a cosmology-independent part, embodied in the effective conductances, that is computationally expensive but can be pretabulated as a function of temperature, and a simple cosmology-dependent part, entering through the departures from Saha equilibrium of $2s$ and $2p$ and temperature differences, which are straightforward to compute for each particular cosmology with the effective multilevel atom method developed in AH10.

Before proceeding further, let us point out that even though we have Taylor-expanded our expressions in the small difference between matter and radiation temperature, this is not required. One can very easily obtain more general expressions for arbitrary $\Delta T/T$, in which the coefficient $d\mathcal{G}^e/d\nu$ would become a function of radiation *and* matter temperatures. We leave it as an exercice for the interested reader to derive the exact expressions.

IV. IMPLEMENTATION AND RESULTS

A. Computation of effective conductances

The computation of the effective conductances requires solving large (formally infinite) linear systems. One must impose some truncation criterion to make the system finite and tractable. Following previous works, we simply ignore all excited levels above some cutoff value of the principal quantum number[4] $n_{\rm max}$.

We tabulated the effective conductances on a grid of temperatures for several values of $n_{\rm max}$ ranging from 60 to 500. Matrix elements for bound-bound transitions were computed as in Ref. [39] and those for free-bound transitions as in Ref. [40]. Equations (26) and (28) for the probabilities $P^i_K(T_{\rm r})$ and the dimensionless numbers $\tilde{P}^e_K(T_{\rm r})$ represent the time consuming part of the problem, as they require solving large (of order $n^2_{\rm max}/2\times n^2_{\rm max}/2$) matrix equations. Due to selection rules for radiative transitions, these large matrices are very sparse, and only have of order $n^3_{\rm max}$ nonvanishing elements. We can therefore use a sparse matrix technique identical to the one introduced in Ref. [38].

We show some of the computed effective conductances in Fig. 2, for a temperature $T_{\rm r} = 3800$ K (corresponding roughly to the peak of the emission).

B. Practical simplification

Equation (39) is a rather remarkable result in its raw form, but its implementation without further simplification could be somewhat cumbersome: if considering excited states up to principal quantum number $n_{\rm max}$, one would in principle need to tabulate of order $n^2_{\rm max}/2$ functions $\mathcal{G}_{n'n}(T_{\rm r})$ as a function of temperature. For $n_{\rm max}$ of a few hundred, required for a fully converged spectrum in the GHz region, one would need to store tens of thousands of coefficients on a fine grid of temperature values, interpolate them at each redshift, and compute the recombination spectrum on a grid fine enough to resolve all the resonances. In addition, whereas hydrogen and singly ionized helium benefit from the accidental energy degeneracy between angular momentum substates, this is not the case for neutral helium, which as a consequence has a much larger set of lines.

In order to save a significant amount of memory with negligible cost in accuracy (as we shall demonstrate in the next section), we group resonances into bins b of finite width $\Delta\nu_b$, so we use

$$\frac{d\mathcal{G}^{e,i}}{d\nu}\Big|_{\rm used} = \sum_b \mathcal{G}^{e,i}_b\delta(\nu-\nu_b), \quad (41)$$

where ν_b are the bin centers, and

$$\mathcal{G}^{e,i}_b \equiv \sum_{n<n'} \mathcal{G}^{e,i}_{n'n}\;\mathbf{1}_b(\nu_{n'n}) + \Delta\nu_b\frac{d\mathcal{G}^{e,i}_{\rm fb}}{d\nu}(\nu_b), \quad (42)$$

where $\mathbf{1}_b(\nu)$ is unity if ν falls inside the bin b and zero elsewhere. The characteristic error resulting from this simplification should be of the order of a few times $\Delta\log\nu_b$, the log-spacing between bins, since the recombination timescale is a few times shorter than the Hubble time[5]. In order to reduce the error induced by this simplification, we enforce that the bin centers coincide with the lowest order transition they may contain (and are logarithmically spaced otherwise). As can be seen

[4] Other truncation schemes could be imagined, such as assuming that the excited states above some threshold are in Saha equilibrium with the continuum; in practice, as long as a clear convergence is exhibited with increasing $n_{\rm max}$, we need not worry about the detailed truncation prescription.

[5] This can be understood from Eq. (13): a fractional error $\Delta\log\nu$ in the rest-frame frequency translates into the same fractional error in the redshift of emission, hence a fractional error $\Delta\log\nu/(H\tau)$ on the emissivity, where $\tau\sim H^{-1}$/few is the characteristic time of evolution of the populations.

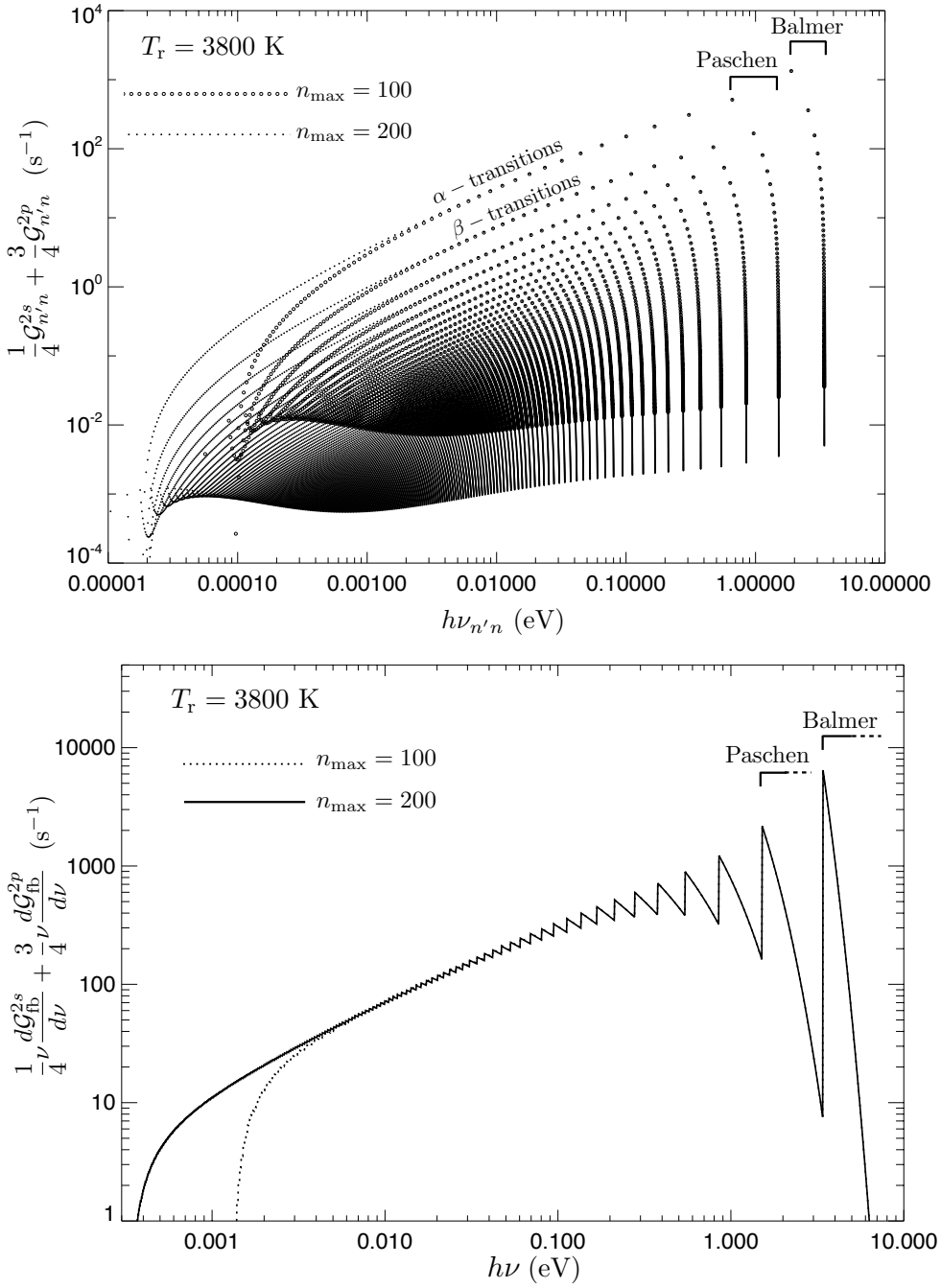

FIG. 2. *Upper panel*: Weighted average of effective conductances $\frac{1}{4}\mathcal{G}^{2s}_{n'n} + \frac{3}{4}\mathcal{G}^{2p}_{n'n}$ at $T = 3800$ K, as a function of transition energy $h\nu_{n'n}$, for $n_{\rm max} = 100$ (open circles) and $n_{\rm max} = 200$ (dots). The nearly vertical families of points correspond to a given series $n' \to n$ with fixed n, such as the Balmer series $n' \to 2$, the Paschen series $n' \to 3$, etc..., with n increasing from right to left. The families of diagonal lines correspond to a given order $(n + \Delta n) \to n$ with fixed Δn, such as the $\alpha-$transitions $(n+1) \to n$, the $\beta-$transitions $(n+2) \to n$ etc..., with lower conductances for higher order transitions. *Lower panel*: Weighted average of effective free-bound conductances per log-frequency interval $\frac{1}{4}\nu\frac{d\mathcal{G}^{2s}_{\rm fb}}{d\nu} + \frac{3}{4}\nu\frac{d\mathcal{G}^{2p}_{\rm fb}}{d\nu}$ at $T = 3800$ K, as a function of photon energy $h\nu$, for $n_{\rm max} = 100$ (dotted line) and $n_{\rm max} = 200$ (solid line). The edges correspond to photoionization thresholds from various shells. We only show the effective conductances for these two values of $n_{\rm max}$ in order not to cluster the figure; proper convergence with $n_{\rm max}$ is discussed in Section IV.

from Fig. 2, effective conductances indeed decrease with increasing transition order (see also Table 1 of Ref. [18]).

With this discretization, the emissivity for bound-bound and free-bound transitions between excited states becomes

$$\frac{1}{n_{\rm H}} j_\nu\big|^{\text{high-}n}_{\text{used}} = \frac{h\nu}{4\pi} \times \sum_b \Big\{ \mathcal{G}^e_b \; n_{\rm H} x_e x_p \frac{\Delta T}{T} - \sum_{i=2s,2p} \mathcal{G}^i_b \; \Delta x_i \Big\} \delta(\nu - \nu_b). \quad (43)$$

C. Lyman-α and $2s-1s$ emission

The net emissivity in the Lyman-α line is given by

$$\frac{j_\nu\big|_{\rm Ly\alpha}}{n_{\rm H}} = \frac{h\nu}{4\pi} \left(x_{2p} - 3 x_{1s} {\rm e}^{-h\nu_{\rm Ly\alpha}/kT_{\rm r}} \right) \times P_{\rm esc} A_{2p,1s} \delta(\nu - \nu_{\rm Ly\alpha}), \quad (44)$$

where $P_{\rm esc}$ is the escape probability for the optically thick Lyman-α line. In the Sobolev approximation (see for example Ref. [41] for a detailed derivation), it is given by

$$P_{\rm esc} = \frac{8\pi H \nu^3}{3c^3 n_{\rm H} x_{1s} A_{2p,1s}}. \quad (45)$$

The $2s-1s$ two-photon emissivity is given by

$$\frac{j_\nu\big|_{2\gamma}}{n_{\rm H}} = \frac{h\nu}{4\pi} \frac{d\Lambda_{2s,1s}}{d\nu} \left[x_{2s}(1+f_{\nu'})(1+f_\nu) - x_{1s} f_{\nu'} f_\nu \right], \quad (46)$$

where $\nu' = \nu_{\rm Ly\alpha} - \nu$ and $f_\nu, f_{\nu'}$ are the values of the photon occupation number at ν, ν'. This expression properly accounts for stimulated decays and absorption of non-thermal photons (emitted in the Lyα line for example). In order to be consistent with our simple "standard" treatment of two-photon decays (see next section), we shall neglect these two effects here and use the approximate expression

$$\frac{j_\nu\big|_{2\gamma}}{n_{\rm H}} \approx \frac{h\nu}{4\pi} \frac{d\Lambda_{2s,1s}}{d\nu} \left[x_{2s} - x_{1s} {\rm e}^{-h\nu_{\rm Ly\alpha}/kT_{\rm r}} \right]. \quad (47)$$

We approximated the differential two-photon decay rate $d\Lambda_{2s,1s}/d\nu$ with the fitting formula of Ref. [42].

Note that neither Eq. (44) nor Eq. (47) are accurate at the percent level. If needed, it would be relatively straightforward to include the appropriate corrections.

D. Fast part of the computation

In this section we briefly recall how the recombination history can be very efficiently computed with the EMLA method [29] and give explicit equations for the "voltages" that source the emissivities.

The EMLA formulation of the problem collapses all the fast and thermally-mediated interior transitions into the effective recombination coefficients $\mathcal{A}_i(T_{\rm m}, T_{\rm r})$, photoionization rates $\mathcal{B}_i(T_{\rm r})$ and transition rates $\mathcal{R}_{i\rightarrow j}(T_{\rm r})$ for $i, j = 2s, 2p$. All the complication of the recombination computation then resides in the slow transitions to the ground state, where a proper time-dependent radiative transfer calculation is required for percent-level precision. Here we are not worried about such subtleties, and use the following simple prescriptions for decay rates to the ground state. For the two-photon transitions from $2s$, we neglect stimulated decays and absorptions of non-thermal photons, so the net decay rate is

$$\dot{x}_{1s}\big|_{2\gamma} = -\dot{x}_{2s}\big|_{2\gamma} = \Lambda_{2s,1s} \left[x_{2s} - x_{1s} {\rm e}^{-E_{21}/kT_{\rm r}} \right], \quad (48)$$

where $\Lambda_{2s,1s} \approx 8.22 \text{ s}^{-1}$ is the spontaneous two-photon decay rate. For the net decay rate in the Lyman-α line, we use the Sobolev approximation,

$$\dot{x}_{1s}\big|_{\rm Ly\alpha} = -\dot{x}_{2p}\big|_{\rm Ly\alpha} = R_{\rm Ly\alpha} \left[x_{2p} - 3 x_{1s} {\rm e}^{-E_{21}/kT_{\rm r}} \right], \quad (49)$$

where $R_{\rm Ly\alpha} \equiv A_{2p,1s} P_{\rm esc}$ is the net decay rate in the Ly-α line, accounting for the small escape probability of resonant photon, given in Eq. (45).

The steady-state rate equations for $2s$ and $2p$ then read

$$0 \approx \dot{x}_{2s} = n_{\rm H} x_e x_p \mathcal{A}_{2s} + x_{1s} {\rm e}^{-E_{21}/kT_{\rm r}} \Lambda_{2s,1s} + x_{2p} \mathcal{R}_{2p\rightarrow 2s} - \Gamma_{2s} x_{2s}, \quad (50)$$

$$0 \approx \dot{x}_{2s} = n_{\rm H} x_e x_p \mathcal{A}_{2p} + 3 x_{1s} {\rm e}^{-E_{21}/kT_{\rm r}} R_{\rm Ly\alpha} + x_{2s} \mathcal{R}_{2s\rightarrow 2p} - \Gamma_{2p} x_{2p}, \quad (51)$$

where the effective inverse lifetimes of the $2s$ and $2p$ states are given by

$$\Gamma_{2s} \equiv \mathcal{B}_{2s} + \mathcal{R}_{2s\rightarrow 2p} + \Lambda_{2s,1s}, \quad (52)$$

$$\Gamma_{2p} \equiv \mathcal{B}_{2p} + \mathcal{R}_{2p\rightarrow 2s} + R_{\rm Ly\alpha}. \quad (53)$$

This simple 2 by 2 system (which is *exact* in the limit that $2s$ and $2p$ are the only interface states) can be solved analytically. Using detailed balance relations satisfied by the effective rates, we find that the departures from Saha equilibrium are given by

$$\Delta x_{2s} = \frac{s_{2s} + s_{2p} \frac{\mathcal{R}_{2p\rightarrow 2s}}{\Gamma_{2p}}}{\Gamma_{2s} - \mathcal{R}_{2s\rightarrow 2p} \frac{\mathcal{R}_{2p\rightarrow 2s}}{\Gamma_{2p}}} \quad (54)$$

$$\Delta x_{2p} = \frac{s_{2p} + s_{2s} \frac{\mathcal{R}_{2s\rightarrow 2p}}{\Gamma_{2s}}}{\Gamma_{2p} - \mathcal{R}_{2p\rightarrow 2s} \frac{\mathcal{R}_{2s\rightarrow 2p}}{\Gamma_{2s}}}, \quad (55)$$

where we have defined

$$s_{2s} \equiv n_{\rm H} x_e x_p \; \Delta\mathcal{A}_{2s} + \Delta x_{1s} \; {\rm e}^{-E_{21}/kT_{\rm r}} \Lambda_{2s,1s}, \quad (56)$$

$$s_{2p} \equiv n_{\rm H} x_e x_p \; \Delta\mathcal{A}_{2p} + 3 \; \Delta x_{1s} \; {\rm e}^{-E_{21}/kT_{\rm r}} R_{\rm Ly\alpha}, \quad (57)$$

where $\Delta\mathcal{A}_i \equiv \mathcal{A}_i(T_{\rm m}, T_{\rm r}) - \mathcal{A}_i(T_{\rm r}, T_{\rm r})$ and Δx_{1s} is the departure of the ground state population from Saha equilibrium with the plasma, defined as in Eq. (4). Similar expressions can easily be obtained for the departures from

Boltzmann equilibrium with the ground state, needed for the Lyman-α and $2s-1s$ emissivities.

The rate of change of the free-electron fraction can be obtained, for example, from the departures from Saha equilibrium computed above:

$$\dot{x}_e = -\sum_{i=2s,2p} \left[n_{\rm H} x_e x_p \Delta\mathcal{A}_i - \Delta x_i \mathcal{B}_i \right]. \quad (58)$$

Finally, the matter temperature is obtained from the Compton-heating equation,

$$\dot{T}_{\rm m} = -2HT_{\rm m} + \frac{8x_e\sigma_{\rm T}a_{\rm r}T_{\rm r}^4}{3(1+x_e+f_{\rm He})m_e c}(T_{\rm r}-T_{\rm m}), \quad (59)$$

where $\sigma_{\rm T}$ is the Thomson cross-section, $a_{\rm r}$ is the radiation constant, m_e is the electron mass and $f_{\rm He}$ is the He:H abundance ratio. At high redshifts where $T_{\rm m}$ is locked to $T_{\rm r}$, one can use the quasi-steady-state solution [37]

$$\frac{\Delta T}{T} \approx \frac{3H(1+x_e+f_{\rm He})m_e c}{8x_e\sigma_{\rm T}a_{\rm r}T_{\rm r}^4}. \quad (60)$$

As an aside, we point out that it is straightforward to include the effect of dark matter annihilations in this system of equations (see for example Refs. [24, 43]). One simply has to add an additional photoionization term to the free-electron fraction evolution equation, a heating term to the matter-temperature evolution equation, and properly account for the additional excitations when solving for the populations of the excited states.

E. Numerical solution of the radiative transfer equation

We first solve for the ionization history and matter temperature as described in Section IV D, using the code HyRec in `EMLA` mode, which we have adapted to also extract the populations of the excited states (more precisely, their departures form equilibrium). We store these quantities on a fine redshift grid ranging from $z = 2500$ to $z = 400$ for future interpolation.

We follow the spectral distortion from $z = 2500$ to $z = 400$ on a constant energy range $10^{-5}{\rm eV} < E < 10.2$ eV, where the upper limit corresponds to the Lyman-α frequency. We assume a purely thermal spectrum blueward of Ly-α. Below $z = 400$, we set the emissivity to zero and freely redshift the distortion down to $z = 0$.

We discretize the $2s-1s$ emissivity on the same grid as the high-n transitions emissivity. Our total discretized emissivity therefore has the form

$$j_\nu\big|_{\rm used} = \sum_b J_b \delta(\nu-\nu_b). \quad (61)$$

At each time step, we first redshift the pre-existing spectral distortion from one bin to the next lower one, using Eq. (12). We then update it by adding the emission from the "lines" at frequencies ν_b, as in Eq. (14). This procedure was used (with additional complications due to large optical depths and frequency diffusion) in Refs. [35, 37]. This method forces the timestep $\Delta\log a$ to be no greater than the smallest bin separation $\Delta\log\nu$.

In our fiducial computation, we have grouped effective conductances in bins of width $\Delta\log\nu = 10^{-2}$ (and we recall that the central frequency assigned to each bin is chosen to coincide with the frequency of the lowest-order line it contains), and used a time-step $\Delta\log a = 5\times10^{-3}$. We have checked that reducing the bin width and timestep by a factor of 10 leads to maximum changes of at most a percent over the whole range of frequencies considered, with a root-mean-square difference of the order of 0.15%. We also checked that the spectrum is converged with respect to the redshift range over which it is computed – this stems from the fact that the emissivities are relatively sharply peaked around $z \sim 1300$, as we show in the next section.

F. Results

All quantities shown in this section are evaluated for a flat universe with fiducial cosmological parameters consistent with the latest WMAP results [1]: $T_{\rm cmb} = 2.728$ K, $\Omega_b h^2 = 0.022$, $\Omega_m h^2 = 0.13$, $\Omega_\Lambda h^2 = 0.34$, $Y_{\rm He} = 0.24$, $N_{\nu,{\rm eff}} = 3.04$.

In Fig. 3, we show the number of photons emitted per hydrogen atom per logarithmic redshift interval or per logarithmic interval of observed frequency, for the first few transitions of the Balmer series, and for the α-transitions of the first few series. We see that in general the number of emitted photons decreases rapidly with the order of the transition within a series, and decreases as well (but less rapidly) for higher series. Note that some transitions may show absorption, as the Hβ transition [18]. We find that a total of 0.63, 0.019, 0.036, 0.32 and 0.13 photons are emitted per hydrogen atom in the Hα, Hβ, Hγ, Pα and Brα transitions, respectively.

Figure 4 shows the convergence of the high-n bound-bound and free-bound spectra with $n_{\rm max}$. We find that the fractional difference in the total spectrum between $n_{\rm max} = 250$ and $n_{\rm max} = 500$ is less than a percent for $\nu \gtrsim 0.5$ GHz. Nothing formally limits us from going beyond $n_{\rm max} = 500$ with our method, since the tabulation of effective conductances needs to be done only once. However, consistently computing the spectrum at low frequencies would also require accounting for free-free absorption and collisional transitions [19, 28], which we do not include here. We therefore limit ourselves to $n_{\rm max} = 500$ for now, keeping in mind that the spectrum obtained is not accurate below a few tenths of GHz.

Figure 5 shows the total recombination spectrum today, as well as its subcomponents: bound-bound, free-bound, two-photon emission from $2s-1s$ decays, and Lyman-α emission. Note that in the present work we have not accounted for any of the radiative transfer effects recently investigated with the purpose of obtaining

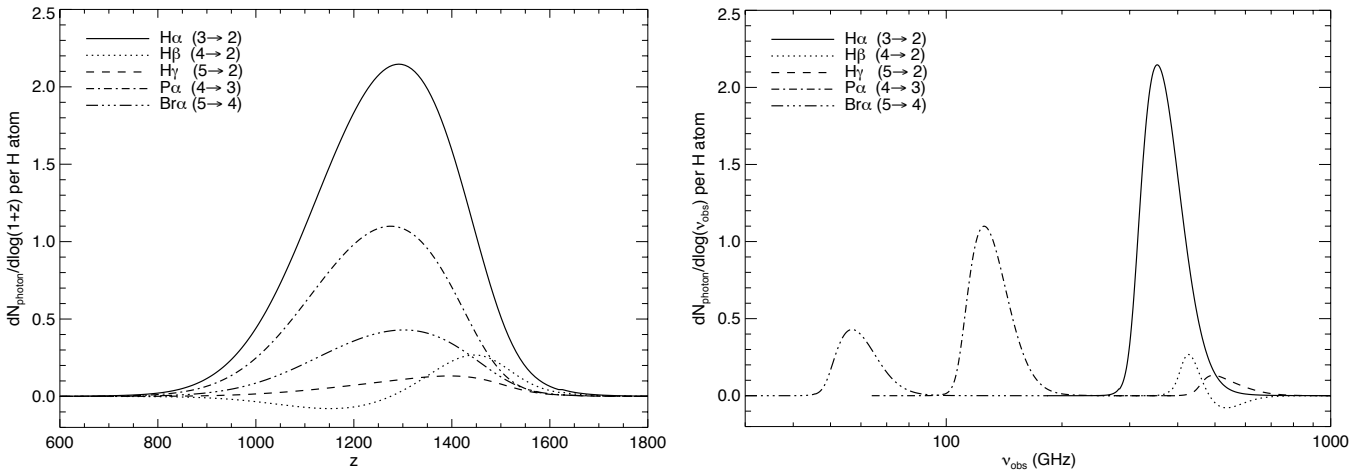

FIG. 3. Number of photons per hydrogen atom emitted per logarithmic redshift interval (or equivalently per logarithmic interval of today's observation frequency), for several bound-bound transitions. In the left panel, this quantity is plotted as a function of emission redshift. In the right panel, it is plotted as a function of observed frequency today. The two are related by $\nu_{\rm obs} = \nu_{\rm em}/(1+z_{\rm em})$.

high-accuracy recombination histories (see for example Refs. [37, 41, 44–49] and many more references therein). It is to be expected that these corrections will lead to a few percent corrections to the recombination spectrum; nevertheless, we are far from even detecting the recombination spectrum, and such refinements are not yet needed for this purpose. The effective conductance method is, moreover, oblivious to all the complications that may occur between interface states and the ground state, and could be very easily adapted to include these effects[6]. If needed for some reason, a high-accuracy Lyman-lines and $2s-1s$ spectrum can be extracted from the modern recombination codes HyRec [35] and CosmoRec[7] [50], that do account for these radiative transfer effects.

Let us point out that even though we have performed all computations with the correct matter temperature, we found that setting $T_{\rm m} = T_{\rm r}$ (and doing so consistently, including when computing the ionization history and departures from Saha equilibrium), leads to an error of at most 0.4% for $\nu \geq 0.1$ GHz. It would therefore be sufficient, at the percent level of accuracy, to assume $T_{\rm m} = T_{\rm r}$ for the spectrum computation (this assumption is not valid if one wishes to compute the low-redshift tail of the recombination history, when the two temperatures may differ significantly).

Finally, we have compared our results with those of Ref. [12] and found a very good agreement. More thorough comparisons will be made once we implement emission from helium as well.

The recurring time for computing a full recombination spectrum, independent of $n_{\rm max}$ used for the effective conductances, is approximately 0.1 second on a standard workstation. This is four to six orders of magnitude faster than the standard multilevel atom method[8], depending on the value used for $n_{\rm max}$ [28].

V. CONCLUSIONS AND FUTURE DIRECTIONS

In this paper we have introduced a new and highly efficient method to compute the primordial recombination spectrum. Our method relies on the factorization of the problem in a computationally expensive but cosmology-independent part and a very fast cosmology-dependent part – the computational efficiency of the latter part is itself due to a similar method of factorization, the effective multilevel atom method, introduced in an earlier work [29]. The recurring cost of a spectrum computation with this method is a fraction of a second, at least four orders of magnitude faster than computations carried out with the standard multilevel atom method.

The computations carried out here relied on several simplifying assumptions. First, we have restricted ourselves to the "standard" (i.e. simplified) transitions from $2s$ and $2p$ to the ground state, and have neglected a whole suite of radiative transfer effects that were shown to be

[6] A subtlety might arise when dealing with two-photon decays from higher levels, as one must avoid double-counting of the low-frequency photons.

[7] http://www.cita.utoronto.ca/∼jchluba

[8] One can speed up the computation of the spectrum by a factor of ~ 10 if precomputing the recombination history with the EMLA method [29] and then computing the spectrum with the standard MLA method but with a larger timestep (J. Chluba, private communication). This would still be a few orders of magnitude slower than the method we present here.

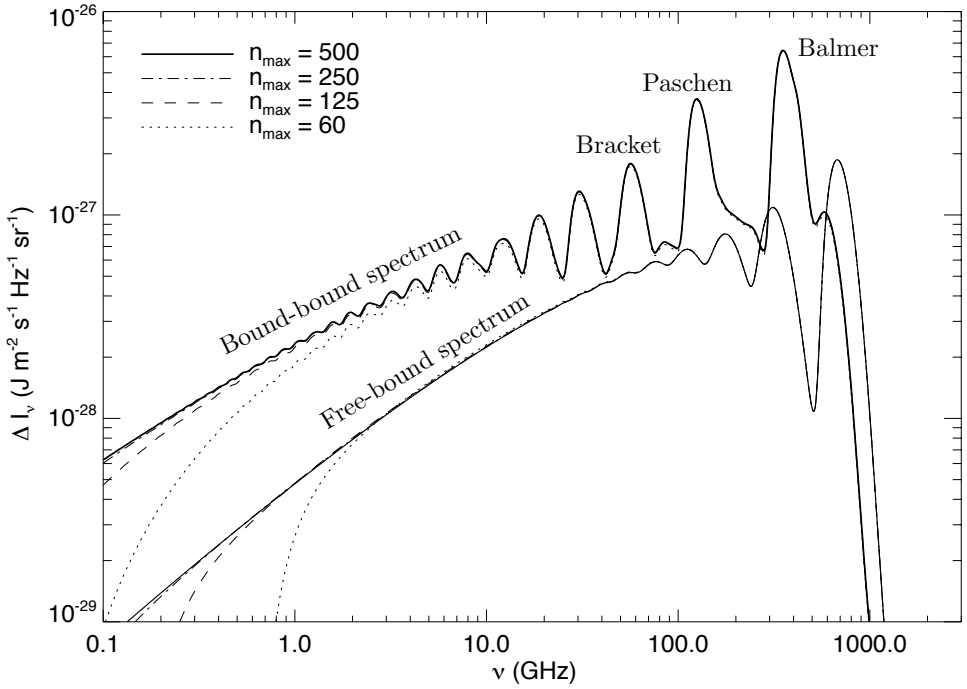

FIG. 4. Bound-bound (*not* including $2s \rightarrow 1s$ and Ly-α photons) and free-bound spectra for various values of the cutoff principal quantum number $n_{\rm max}$.

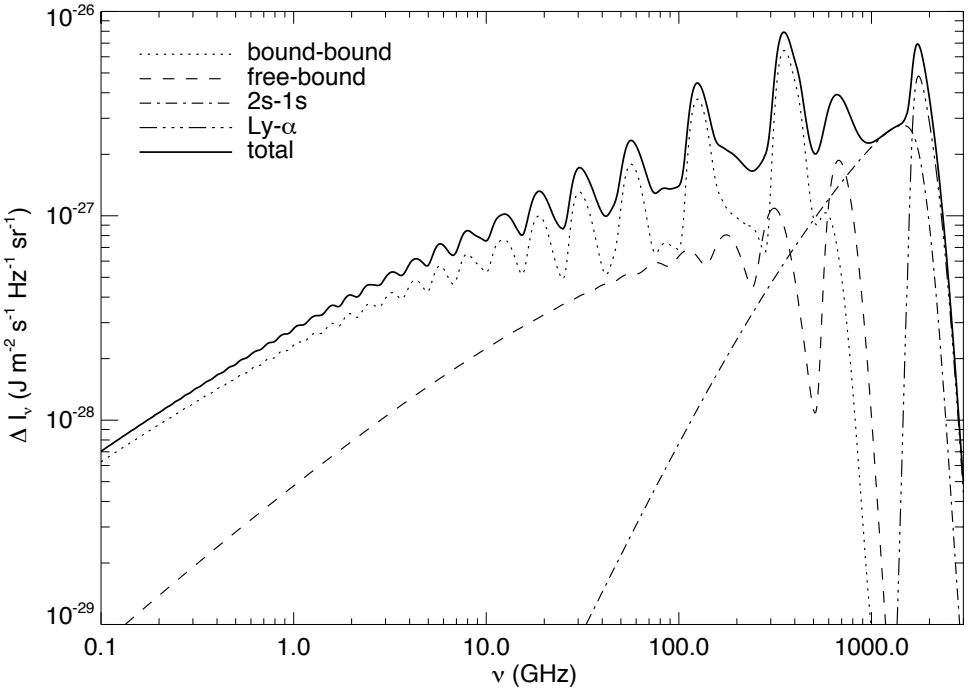

FIG. 5. Total spectral distortion created by hydrogen emission (neglecting the influence of helium), as well as individual contributions from various processes, using $n_{\rm max} = 500$. The "bound-bound" curve only accounts for $n' \rightarrow n \geq 2$ transitions. We display ΔI_ν in the same units as Refs. [12, 18] for an easier comparison by eye.

important for a highly accurate recombination history and are efficiently computed by modern recombination codes [35, 50]. To our knowledge, no computation of the primordial recombination spectrum thus far has also included all these effects consistently. Including them with our formalism should not raise any major issues, but they are expected to induce corrections to the spectrum at the level of a few percent at most (though in principle one should check this statement precisely). The second aspect we neglected is collisional transitions. They were shown to modify the spectrum mostly in the low frequency regime $\nu \lesssim 0.1$ GHz, where the recombination distortions are very smooth and therefore probably difficult to observe [28]. Finally, we neglected broadening of the lines by electron scattering, as well as free-free absorption. The former effect should increase the width of the broad spectral features by less than a percent of their central frequency, and the latter strongly affects the spectrum at frequencies below ~ 0.1 GHz [19]. Since all these effects are small in the frequency regime $\nu \gtrsim 0.1$ GHz, we do not consider them a priority before the observability of the recombination spectrum is solidly established.

In this work we have only dealt with the line and continuum emission from recombining hydrogen atoms, and have neglected the effect of helium on the recombination spectrum (but we did account for helium when computing the ionization history of the plasma). The presence of about 0.08 helium nuclei per hydrogen nucleus will modify our results in the two following ways. First, photons emitted in the HeI $2^1\mathrm{P}-1^1\mathrm{S}$ line (the equivalent of the hydrogen Ly-α line) with an energy of 21.2 eV can photoionize some of the few neutral hydrogen atoms already present at the epoch of HeII$\rightarrow$ HeI recombination [51–54]. This effect is already included in our code when computing the ionization fraction of helium [35], but we have not accounted here for the small departure from Saha equilibrium that it induces for hydrogen, and the resulting line emission. This process was studied in detail in Ref. [54], who showed that it leads to pre-recombination emission features in the hydrogen spectrum. Inclusion of this effect with our method presents no additional complication: one only needs to properly compute the small departures from equilibrium in hydrogen, given the helium ionizing photons. The second and more direct consequence of having helium nuclei is that they too recombined, and in the process, emitted a few nonthermal photons per helium nucleus. Because helium recombined in two stages (at redshifts $z \sim 6000$ for HeIII$\rightarrow$ HeII recombination and $z \sim 2000$ for HeII$\rightarrow$ HeI recombination), this results in ~ 0.16 helium recombination photons per hydrogen recombination photon, which is a non-negligible contribution to the spectrum, and can be used to probe the primordial helium abundance before the first stars formed [20]. Computing the emission from helium recombination can be achieved with the exact same method, the only additional work would be to compute effective conductances for HeI (those for HeII can be easily obtained from the ones computed for hydrogen by simple rescalings). Such additions are essential and we shall include them in the near future.

An additional aspect that we have not treated here is the processing of pre-existing spectral distortions by the recombining atoms. These can lead to large enhancements of the line emission, even if the initial smooth spectral distortion is tiny [23]. Formally, one can generalize our method to account for non-thermally mediated transitions, as long as the underlying spectrum can be described by a small set of parameters. We defer such a study to future work. Once the latter two aspects are implemented, we shall release a public code to efficiently compute the recombination spectrum.

Besides having a certain aesthetic appeal, we believe that the factorization method presented here will prove very useful in order to quantitatively study the information content of the recombination spectrum. Most of our knowledge about the early universe currently comes from the study of *spatial* variations of the thermal photon background, through CMB anisotropy observations. An exciting avenue is to probe the *spectral* variations of the CMB, which might inform us about the universe before the last-scattering redshift. A fast and accurate code to compute the primordial spectrum will be of great help to study precisely if, what and how new information can be gained from the primordial spectrum.

ACKNOWLEDGMENTS

I thank Chris Hirata for pointing out the analogy of the system of fast high-n transitions with a circuit. I am grateful to Jens Chluba for providing recombination spectra for comparison with the results presented here and to Matias Zaldarriaga for discussions on this work. I am indebted to Simeon Bird, Jens Chluba and Daniel Grin for reading the draft of this manuscript and providing many useful comments. This work was completed at the Institute for Advanced Study with the support of the National Science Foundation grant number AST-0807444 and the Frank and Peggy Taplin Membership. I also acknowledge support from Rashid Sunyaev at the Max Planck Institute for Astrophysics during part of summer of 2012, when the first steps of this study were taken.

[1] E. Komatsu *et al.*, Astrophys. J. Suppl. Ser. **192**, 18 (2011), arXiv:1001.4538 [astro-ph.CO].

[2] R. A. Sunyaev and Y. B. Zeldovich, Comments on Astrophysics and Space Physics **2**, 66 (1970).

[3] R. A. Sunyaev and J. Chluba, Astronomische Nachrichten **330**, 657 (2009), arXiv:0908.0435 [astro-ph.CO].

[4] R. Khatri and R. A. Sunyaev, J. Cosm. Astropart. Phys. **9**, 016 (2012), arXiv:1207.6654 [astro-ph.CO].

[5] W. Hu, D. Scott, and J. Silk, Astrophys. J. Lett. **430**, L5 (1994), arXiv:astro-ph/9402045.

[6] W. Hu and J. Silk, Phys. Rev. D **48**, 485 (1993).

[7] J. Chluba, R. Khatri, and R. A. Sunyaev, Mon. Not. R. Astron. Soc. **425**, 1129 (2012), arXiv:1202.0057 [astro-ph.CO].

[8] E. Pajer and M. Zaldarriaga, ArXiv e-prints (2012), arXiv:1206.4479 [astro-ph.CO].

[9] P. J. E. Peebles, Astrophys. J. **153**, 1 (1968).

[10] Y. B. Zel'dovich, V. G. Kurt, and R. A. Syunyaev, Soviet Journal of Experimental and Theoretical Physics **28**, 146 (1969).

[11] D. J. Fixsen, E. Dwek, J. C. Mather, C. L. Bennett, and R. A. Shafer, Astrophys. J. **508**, 123 (1998), arXiv:astro-ph/9803021.

[12] J. Chluba and R. A. Sunyaev, Astron. Astrophys. **458**, L29 (2006), arXiv:astro-ph/0608120.

[13] V. K. Dubrovich, Soviet Astronomy Letters **1**, 196 (1975).

[14] I. N. Bernshtein, D. N. Bernshtein, and V. K. Dubrovich, Sov. Astron. **21**, 409 (1977).

[15] Y. E. Lyubarsky and R. A. Sunyaev, Astron. Astrophys. **123**, 171 (1983).

[16] G. B. Rybicki and I. P. dell'Antonio, in *Observational Cosmology*, Astronomical Society of the Pacific Conference Series, Vol. 51, edited by G. L. Chincarini, A. Iovino, T. Maccacaro, and D. Maccagni (1993) p. 548.

[17] M. S. Burgin, Astronomy Reports **47**, 709 (2003).

[18] J. A. Rubiño-Martín, J. Chluba, and R. A. Sunyaev, Mon. Not. R. Astron. Soc. **371**, 1939 (2006), arXiv:astro-ph/0607373.

[19] J. Chluba, J. A. Rubiño-Martín, and R. A. Sunyaev, Mon. Not. R. Astron. Soc. **374**, 1310 (2007), arXiv:astro-ph/0608242.

[20] J. A. Rubiño-Martín, J. Chluba, and R. A. Sunyaev, Astron. Astrophys. **485**, 377 (2008), arXiv:0711.0594.

[21] D. J. Fixsen, E. S. Cheng, J. M. Gales, J. C. Mather, R. A. Shafer, and E. L. Wright, Astrophys. J. **473**, 576 (1996), arXiv:astro-ph/9605054.

[22] J. Chluba and R. A. Sunyaev, Astron. Astrophys. **478**, L27 (2008), arXiv:0707.0188.

[23] J. Chluba and R. A. Sunyaev, Astron. Astrophys. **501**, 29 (2009), arXiv:0803.3584.

[24] J. Chluba, Mon. Not. R. Astron. Soc. **402**, 1195 (2010), arXiv:0910.3663 [astro-ph.CO].

[25] A. Kogut, D. J. Fixsen, D. T. Chuss, J. Dotson, E. Dwek, M. Halpern, G. F. Hinshaw, S. M. Meyer, S. H. Moseley, M. D. Seiffert, D. N. Spergel, and E. J. Wollack, J. Cosm. Astropart. Phys. **7**, 025 (2011), arXiv:1105.2044 [astro-ph.CO].

[26] W. A. Fendt, Jr., *Precision cosmological parameter estimation*, Ph.D. thesis, University of Illinois at Urbana-Champaign (2009).

[27] W. A. Fendt and B. D. Wandelt, Astrophys. J. **654**, 2 (2007), arXiv:astro-ph/0606709.

[28] J. Chluba, G. M. Vasil, and L. J. Dursi, Mon. Not. R. Astron. Soc. **407**, 599 (2010), arXiv:1003.4928 [astro-ph.CO].

[29] Y. Ali-Haïmoud and C. M. Hirata, Phys. Rev. D **82**, 063521 (2010), arXiv:1006.1355 [astro-ph.CO].

[30] M. S. Burgin, Bulletin of the Lebedev Physics Institute **36**, 110 (2009).

[31] M. S. Burgin, Bulletin of the Lebedev Physics Institute **37**, 280 (2010).

[32] C. M. Hirata, blackboard conversation (2010).

[33] U. Seljak and M. Zaldarriaga, Astrophys. J. **469**, 437 (1996), arXiv:astro-ph/9603033.

[34] S. Seager, D. D. Sasselov, and D. Scott, Astrophys. J. Suppl. Ser. **128**, 407 (2000), arXiv:astro-ph/9912182.

[35] Y. Ali-Haïmoud and C. M. Hirata, Phys. Rev. D **83**, 043513 (2011), arXiv:1011.3758 [astro-ph.CO].

[36] G. B. Rybicki and A. P. Lightman, *Radiative Processes in Astrophysics, by George B. Rybicki, Alan P. Lightman, pp. 400. ISBN 0-471-82759-2. Wiley-VCH , June 1986.* (1986).

[37] C. M. Hirata, Phys. Rev. D **78**, 023001 (2008), arXiv:0803.0808.

[38] D. Grin and C. M. Hirata, Phys. Rev. D **81**, 083005 (2010), arXiv:0911.1359 [astro-ph.CO].

[39] J. D. Hey, Journal of Physics B Atomic Molecular Physics **39**, 2641 (2006).

[40] A. Burgess, Mem. R. Astr. Soc. **69**, 1 (1965).

[41] Y. Ali-Haïmoud, D. Grin, and C. M. Hirata, Phys. Rev. D **82**, 123502 (2010), arXiv:1009.4697 [astro-ph.CO].

[42] H. Nussbaumer and W. Schmutz, Astron. Astrophys. **138**, 495 (1984).

[43] G. Giesen, J. Lesgourgues, B. Audren, and Y. Ali-Haïmoud, ArXiv e-prints (2012), arXiv:1209.0247 [astro-ph.CO].

[44] J. Chluba and R. A. Sunyaev, Astron. Astrophys. **446**, 39 (2006), arXiv:astro-ph/0508144.

[45] E. E. Kholupenko and A. V. Ivanchik, Astronomy Letters **32**, 795 (2006), arXiv:astro-ph/0611395.

[46] S. I. Grachev and V. K. Dubrovich, Astronomy Letters **34**, 439 (2008), arXiv:0801.3347.

[47] J. Chluba and R. A. Sunyaev, Astron. Astrophys. **480**, 629 (2008), arXiv:0705.3033.

[48] J. Chluba and R. A. Sunyaev, Astron. Astrophys. **503**, 345 (2009), arXiv:0904.2220 [astro-ph.CO].

[49] C. M. Hirata and J. Forbes, Phys. Rev. D **80**, 023001 (2009), arXiv:0903.4925 [astro-ph.CO].

[50] J. Chluba and R. M. Thomas, Mon. Not. R. Astron. Soc. **412**, 748 (2011), arXiv:1010.3631 [astro-ph.CO].

[51] W. Hu, D. Scott, N. Sugiyama, and M. White, Phys. Rev. D **52**, 5498 (1995), arXiv:astro-ph/9505043.

[52] E. E. Kholupenko, A. V. Ivanchik, and D. A. Varshalovich, Mon. Not. R. Astron. Soc. **378**, L39 (2007), arXiv:astro-ph/0703438.

[53] E. R. Switzer and C. M. Hirata, Phys. Rev. D **77**, 083006 (2008), arXiv:astro-ph/0702143.

[54] J. Chluba and R. A. Sunyaev, Mon. Not. R. Astron. Soc. **402**, 1221 (2010), arXiv:0909.2378 [astro-ph.CO].